Pressure-induced transition from wavy circular to ring-shaped buckles

Sen-Jiang Yu, Guillaume Parry, Christophe Coupeau, Lingwei Li

Pressure-induced transition from wavy circular to ring-shaped buckles

Sen-Jiang Yu[a], Guillaume Parry[b], Christophe Coupeau[c,*], Lingwei Li[a,**]

[a]*Key Laboratory of Novel Materials for Sensor of Zhejiang Province, Institute of Advanced Magnetic Materials, Hangzhou Dianzi University, Hangzhou 310012, PR China*

[b]*SIMaP, UMR 5266 CNRS, Université de Grenoble-Alpes, Grenoble 38000, France*

[c]*Institut Pprime, Dpt of Physics and Mechanics of Materials, UPR 3346 CNRS-ENSMA-Université de Poitiers, 86000 Poitiers, France*

[*]Corresponding author: christophe.coupeau@univ-poitiers.fr

[**]Corresponding author: lingwei@hdu.edu.cn

Abstract. We report on buckling structures observed on tantalum films deposited by sputtering on silicon wafers. It is shown that, above a critical diameter, the circular blisters evolve to ring-shaped buckles, whatever the smooth or undulating type of their edges. The experimental results have been compared to finite element simulations. In particular, the polygonal collapsed part at the center of the buckles can be well understood by taking into account the pressure mismatch between the inside and outside parts of the buckles.

Keywords: Thin film; Circular blister; Ring-shaped buckle; Delamination; Stress

1. Introduction

Thin films and coatings have found widespread technological applications, for instance in optics, microelectronics or microfluidics. Residual stresses are of prime importance to ensure the mechanical stability of the coated substrates and further their lifetime. These stresses may result from different origins, such as the deposition process of the filmitself, the lattice mismatch between the film and its associated substrate, the discrepancy between the thermal expansion coefficients of the film and the substrate, an external mechanical loading, implantation/irradiation processes or environmental parameters like moisture. If the stress is compressive and high enough and if the interface adhesion is comparatively weak, the film may delaminate from its substrate and release the stored elastic energy by buckling, leading to various complex morphologies among which elementary buckles are the straight-sided (SS) (Audoly et al., 2002; Coupeau et al., Pundt et al., 2003; 2004; Yu et al., Cordill et al. 2010; Jin et al. 2011; 2014; Kleinbichler et al., 2018; Coupeau et al., 2019;), the circular buckles (CB) (Gioia et al., 1997; Wang et al., 1998; Moon et al., 2002a; Moon et al., 2004; McDonald et al. 2006; Lamri et al., 2010; Kuznetsov et al., 2012; Chen et al. 2013; Eren et al., 2014 ; Guo et al., 2017) or the telephone cord (TC) structures (Yu et al., 1991; Moon et al., 2002a; Volinsky, 2003; Cordill et al., 2007; Abdallah et al., 2006; Abdallah et al., 2008; Peponas et al. 2008; Yu et al. 2009; Grachev et al., 2010; Faou et al., 2012; Yu et al., 2014; Marot et al., 2016; Ni et al., 2017). Note that the TC buckles are the most frequently observed due to the isotropic character of the compressive stresses in most of thin films and coatings (Parry et al., 2006). On the other hand, the circular blister usually forms at the early stage of buckling, for instance from film imperfections (Moon et al., 2002b), triggered by indentation (Volinsky et al., 2002) or induced by humidity (Moller et al., 2002; Waters et al., 2007). During its growth, its circular edge is destabilized and forms as a result a petal-like pattern all round its circumference (Argon et al., 1989; Hutchinson et al., 1992a; Lee et al., 2010; Yan et al., 2012). In particular, it was found by finite elements simulations that the period of the undulating edge decreases with the increasing buckle diameter and with the decreasing

film thickness. The axisymmetric growth of the circular blister is thus broken and the petals will gradually evolve to TC buckles, finger branches or complete delamination of the film from its substrate (Faou et al., 2017). Recently, another fascinating buckles, called ring-shaped structure, have been reported in two independent works. Zhou et al. observed ring-shaped and arc-shaped buckles in cobalt films deposited on glass substrates, which are attributed to the coffee ring effect by evaporation of silicone oil (Zhou et al., 2018). On the other hand, Hamade et al. observed donut- and croissant-like buckles in gold films deposited on silicon substrates. They attributed such buckles to the coupling effect of the external/internal pressure mismatch and the plastic folding of the film (Hamade et al., 2015). However, many questions are still open on these specific buckling structures. For instance, the observed ring-shaped buckles exhibit smooth edges (Hamade et al., 2015; Zhou et al., 2018) while larger circular blisters usually have wavy edges (Hutchinson et al., 1992a). The dynamic process of the formation of ring-shaped buckles is also unrevealed up to now.

In this paper, we report on buckling structures experimentally observed by optical and atomic force microscopies on tantalum films deposited by a sputtering method on silicon wafers. The spontaneous transition from circular to ring-shaped buckles is clearly evidenced experimentally, whatever the edge type of the circular blisters, smooth or wavy. The experimental observations are then compared to finite elements method simulations in order to have a better understanding of the physical parameters controlling this transition.

2. Experimental results

The tantalum films were deposited on silicon wafers by direct current magnetron sputtering technique at room temperature. The silicon wafers with 10×10 mm^2 size were washed in ethyl alcohol for 10 min and then in deionized water for another 10 min with ultrasound. The tantalum target was 60 mm in diameter and 3 mm in thickness. The distance from target to substrate was about 80 mm. The base vacuum was prior to 2×10^{-4} Pa and then pure argon gas was filled into the chamber with the pressure of 0.5 Pa. The

sputtering power was 50 W and the deposition time was 8 minutes. The film thickness, measured by a focused ion beam (FIB 200) and a stylus profiler (Dektak XT, Bruker), was estimated to h = 240 nm. The buckle morphologies were investigated by optical microscopy (Leica DMLM) and scanning electron microscopy (SEM, Zeiss Supra 55). The 3D structures of buckles were determined by atomic force microscopy (AFM, Dimension 3100, Veeco) operated in tapping mode under atmospheric conditions.

The surfaces of the as-prepared Ta thin films were initially smooth but buckling structures spontaneously form under ambient conditions while time is running (sometimes several months after), as shown in Fig. 1a. The frequently observed straight-sided and telephone cord buckles have been extensively studied in the past decades. We focused our attention in the following on the axi-symmetrical ones, especially the ring-shaped structures. The typical blisters investigated by optical microcopy are presented in Fig. 2, for various increasing diameters D. Circular blisters are observed for small diameters (Fig. 2a), lower than approximately D^{ring}~70 µm, up to which ring-shaped buckles are observed (Fig. 2b). Note that circular blisters and ring-shaped buckles are both observed in our experiment for D ranging from 70 to 110 µm. In addition, the circular blisters exhibit smooth edges when their diameter is small while wavy edges may be observed (Fig. 2c) above a diameter higher than approximately D^{wavy}~40 µm, leading to a petal-like pattern. Note again that circular blisters with and without edge instability are observed in our experiment in a specific D domain ranging from 40 to 60 µm. Some non-symmetrical (croissant-like) blisters with undulating edges are also sometimes observed (see Fig. 2d-f). At higher diameters, the two phenomena (undulating borders and pushing down in the middle) are combined leading to wavy ring-shaped buckles (see Fig. 2g-i). Finally, a spalling of the Ta film occurs for diameters higher than approximately $D^{spalling}$~160 µm. It has been evidenced (not shown here for convenience) by a focused ion beam milling and scanning electron microscopy investigations that the delamination occurs at the interface between the Ta film and the silicon substrate.

The ring-shaped buckles were already reported by the past and result from a collapse of the thin film at their center, down to the substrate. It was demonstrated by finite elements method (FEM) simulations that the outside atmospheric pressure and plasticity at their circumference are the key parameters explaining their formations (Hamade et al., 2015). An experimental proof of this spontaneous morphological transition is shown in Fig. 3. It is noticed that the edge instability is unchanged during the collapse process. Note also that some buckles are sometimes superimposed one on top of the other, for both the circular and the ring-shaped blisters (see Fig. 1b). It may be interpreted as the signature of plasticity (Coupeau et al., 2003; Cordill et al., 2005) occurring during the buckling-induced delamination process in the Ta films. From a kinetic point of view, the latter case also suggests that, surprisingly, a circular blister may grow by radial delamination even if the edge instabilities already developed at their circumference before. Wavy ring-shaped buckles were almost never mentioned in the literature; one can note the work of (Lee et al., 2010) who reported the collapse of 100 nm thick amorphous Si pressurized blisters. In this work, the gaz and liquid initially inside the circular blisters had diffused out during 24h leading to their collapse to wavy ring-shape blisters. Finally, in the case of ring-shaped buckles with smooth edges previously reported in the literature (Hamade et al., 2015; Zhou et al., 2018), the middle internal part pressed down to the substrate was observed to be quite circular. Surprisingly, the wavy ring-shaped buckles exhibit a polygonal area at their middle, as shown in Fig. 2g-i.

Circular blisters without wavy edges have been studied by using the Föppl-von Karman equations in the framework of the continuum elastic theory. In the elastic buckling model, the blister is treated as a clamped circular elastic plate submitted to an in-plane isotropic compressive stress σ_0. No effect of the substrate is here considered, assumed as elastically hard compared to the film. In this case, the critical stress σ_c for buckling to occur is given by (Yu et al., 1991; Evans et al., 1984; Hutchinson et al., 1992a; Hutchinson et al., 1992b; Lamri et al., 2010; Chen et al. 2013; Eren et al., 2014; Guo et al., 2017):

$$\sigma_c = 1.2235 \frac{E}{1-\nu^2}\left(\frac{2h}{D}\right)^2, \quad (1)$$

with E and ν, the elastic modulus and Poisson's ratio of the film, respectively.

The maximum deflection δ can be expressed by (Hutchinson et al., 1992a; Hutchinson et al., 1992b; Chen et al. 2013, Guo et al., 2017):

$$\delta/h = \frac{1}{c_1}\sqrt{\frac{\sigma_0}{\sigma_c} - 1}, \quad (2)$$

with $c_1 = 0.2473(1+\nu)+0.2231(1+\nu^2)$. For $E_{Ta} = 186$ GPa and $\nu_{Ta} = 0.35$, it leads to $c_1 \sim 0.58$. As $h << \delta$, σ_0 can be expressed from Eqs. (1) and (2) by:

$$\sigma_0 = \frac{1.2235}{c_1}\frac{E}{1-\nu^2}\left(\frac{\delta}{D}\right)^2. \quad (3)$$

The morphological parameters, *i.e.* the maximum deflection δ and the diameter D, have been determined by AFM. The δ/D ratio has been reported in Fig. 4a for various increasing D. It is shown that δ/D does not significantly depend on the blister size, allowing to estimate the internal stress to be constant and approximately equal to $\sigma_0 = 1.4$ GPa in compression.

The petal number N has been reported in Fig. 4b as a function of the diameter D, for both the circular and the ring-shaped buckles. For the circular blisters, it is shown that N increases step-by-step with the increase of D. Similar trends have been experimentally observed by the past, for instance on mica films (Hutchinson et al., 1992a), boron nitride (Moller et al, 2002) or amorphous silicon films (Lee et al., 2010; Yan et al., 2012). In the case of buckling-driven delamination (Hutchinson et al., 1992a), such an incremental increase of N was predicted in the framework of an elastic modeling taking into account a sinusoidal perturbation at the circular crack front (Hutchinson et al., 1992a). In (Lee et al., 2010), the loading configuration of the blisters was also different from ours, as the deflection was predominantly caused by pressure due to the underlying gaseous and liquid droplets inside the blisters rather than internal stresses. This pressure caused membrane tension in the film, the wavelength of the

wrinkles forming around the blister being then computed from a minimization of the bending transverse to the folds and the stretching along their length. In contrast, in our configuration, the buckling is clearly due to compressive internal stresses and the pressure mismatch is reversed, *i.e.* a smaller pressure underneath the blister compared to the outside room pressure. In (Yan et al., 2012), model of circular plate submitted to compressive stress is used, but the difference of pressure underneath and above the blister is not accounted for. One consequence is that the whole family of ring-shaped blister is not present among the computed solutions. It is however worth noting that some of their numerical solutions are close to ours when we will consider small pressure mismatches in our FEM simulations in the following.

Once the circular blisters evolve to ring-shaped buckles, N still increases with the increasing D, even if the incremental increase is no more clearly distinguishable. It suggests that the wavy edge destabilization does not depend on the shape of the buckles, circular or ring-shaped. The wavy blisters have been also characterized by the average period λ of the undulation along their circumferences defined as $\lambda = \pi D/N$. λ presented in Fig. 4c as a function of D, for both the circular and the ring-shaped buckles. Two different behaviors are evidenced: λ steadily decreases for small diameters while it is almost constant for large diameters above 80 µm. The transition seems to be related to the type of buckles, the first (*resp*. the second) regime being associated with the circular blisters (*resp*. the ring-shaped buckles). It strongly suggests that the edge destabilization occurring around circular blisters when the diameter is increased does not follow similar mechanisms once the circular blisters have evolved to ring-shaped buckles.

3. FEM simulations

The simulation box, depicted in Fig. 5, has the shape of a square with edge length L=3D, where D is the circular blister diameter. In order to describe the effect of pressure on the post-buckling regime of the circular blister, a geometrically nonlinear plate model is used in order to describe the thin film. The substrate surface is represented by

a rigid plane forbidding the displacement of the plate in the lower half-space (unilateral contact condition). Hence, the elastic deformation of the substrate is not considered. The whole film, including the circular domain of diameter *D* where the blister is going to develop, is originally in a planar state with its bottom plane located at the substrate surface. The direction normal to the substrate surface is denoted by (Oz). The displacement components along the axes parallel to $\vec{e}_x$, $\vec{e}_y$, and $\vec{e}_z$ are respectively denoted *u*, *v*, and *w*, for any point M(*x*,*y*) of the midplane of the plate. The following boundary conditions are imposed: whatever M outside of the disk of diameter *D*, $u(M)=v(M)=w(M)=0$. This region will be mentioned as 'the bonded part' of the film in the following. In contrast, the region of the disk will be called 'the debonded part'. A rigid contact definition is used between the bottom of the circular patch of plate (free film) and the underneath rigid plane (substrate).

The various buckling patterns are characterized by large values of the out-of-plane displacement component *w*, such that the calculations must be carried out within the framework of large displacement hypothesis using the Green-Lagrange strain tensor. The plate is submitted to two successive loading steps:

- Step 1: Application of the internal stress.

A thermal dilatation strain ε_0 ($\varepsilon_0>0$) is imposed to the film. As the displacement is blocked in the bonded part of the film, the eigenstrain ε_0 generates a compressive stress in the film (because the total strain, which is the sum of the thermal and elastic strains, vanishes), such that $\sigma_{xx}=\sigma_{yy}=-E.\varepsilon_0/(1-\nu)\equiv-\sigma_0$ (with $\sigma_0>0$) and $\sigma_{xy}=0$. This stress state is generated in the bonded part of the film, but also in the debonded part of the film (the circular patch of diameter *D*) as long as it is remaining planar. Note that the eigenstrain is maintained during the next step.

- Step 2: Application of the pressure.

A uniform pressure Δp is applied, onto the upper surface of the buckled film. The equilibrium can be dramatically modified by this loading, leading to secondary buckling equilibria shapes quite different from the original circular shape in the

postcritical regime.

In order to carry out these nonlinear calculations, finite elements simulations have been performed using the software ABAQUS. Quadrilateral shell elements have been used to mesh the film. The element sizes have been chosen in such a way that 40 elements are considered into the film along the diameter. A quasi-static analysis is carried out using the explicit solver. As a matter of fact, due to the presence of two sources of non-linearities (contact and large displacements), an explicit algorithm is preferred to an implicit one even if the analysis is quasi-static. This approach is commonly adopted, imposing for parameters to be chosen carefully so that the kinetic energy always remains very small compared to the strain energy in the elements.

Our study was focused in the following to the case of a Ta film of thickness h = 240 nm, with E = 186 GPa and v = 0.35. For convenience, D was first fixed to 120 µm. The stable shape of the circular plate is shown in Fig. 6, as a function of both the internal compressive stress σ_0 and the pressure mismatch Δp between the outside and inside parts of the buckle. The case Δp=0 corresponds to the case of an atmospheric pressure inside (*i.e*. a non-airtight buckle). In this case, only wavy buckles are energetically stable. As described previously, the number of petals N gradually increases with the increase of σ_0. Increasing Δp leads to the destabilization of the wavy buckles. For high σ_0 values, a ring-shaped buckle is observed. The middle part of the circular plate is now in contact with its substrate and adopts a polygonal shape, whose number of sides increases with Δp. For instance, at σ_0 = 2.5 GPa, a triangle, a square and finally a pentagon is successively observed for Δp = 1, 2 and 4 atm respectively. In addition, the type of polygons significantly modifies the shape of the wavy borders. Some 'mexican-hat' undulations are thus observed for triangles or squares. For low stress values, non axi-symmetrical shapes are evidenced. Among the various complex structures, one can note the horseshoe-like (see Δp = 1 atm and $\sigma_0 \leq$ 1.0 GPa) and the bone-like (see $\Delta p \geq$ 2 atm and σ_0 = 0.5 GPa) patterns.

It was experimentally demonstrated by the past that a pressure may exist inside the circular blisters, for instance induced by a gaseous environment (Parry et al., 2011;

Coupeau et al., 2013) or associated with liquid droplets (Lee et al., 2010), so that $\Delta p<0$. A low vacuum pressure may also exist inside closed-airtight buckles (Coupeau et al., 2010). From an experimental point of view, Δp may thus also range from 0 to 1. In the following, we restricted our study to the ideal case of $\Delta p = 1$ atm, which means vacuum inside and atmospheric outside. The morphological mapping of the circular plate is shown in Fig. 7, as a function of the normalized stress σ_0/E and the normalized diameter D/h. Circular buckles are still present, but only for low σ_0 and low D. As already mentioned previously, increasing σ_0 results in the destabilization of the blister boundaries. No significant pressure effect is consequently observed for low D, *i.e.* no collapse of the blister. When D is increased, the wavy buckles stay energetically favorable, but only for high σ_0 values. At a given stress, the number of petals also increases with increasing D or decreasing h. This behavior is similar to what has been experimentally observed on amorphous Si films, even if it was for pressurized blisters, *i.e.* for $\Delta p<0$ (Lee et al., 2010). The stability domain of the wavy ring-shaped buckles is observed for high diameters, whatever the normalized stress ranging here from approximately 5.10^{-3} to 13.10^{-3}. As experimentally evidenced, the side number of the central polygon decreases with the increasing stress at a given D (see the line at D/h=800). Finally, an intermediate domain is observed at low stresses and medium diameters, for which the bone-like and the horseshoe-like patterns are stable. Note here that the horseshoe-like buckle may exhibit both smooth (see $\sigma_0/E = 2.7\ 10^{-3}$ and $D/h = 500$) and wavy (see $\sigma_0/E = 8.1\ 10^{-3}$ and $D/h = 450$) edges.

The internal stresses in the Ta films were estimated to be 1.4 GPa in compression, which leads to $\sigma_0/E = 7.10^{-3}$. It is expected from Fig. 7 the successive observations of wavy buckles, horseshoe-like and ring-shaped buckles while the diameter D is increased. In addition, the polygon in the middle of the ring-shaped should increase its number of sides. These numerical results are in pretty good agreements with our experimental optical investigations for which the normalized diameters D/h are ranging approximately from 150 to 650 (see Fig. 4b).

Some additional experimental results are shown in Fig. 8. The investigations by AFM were carried out on Mo 200 nm thick films deposited by a sputtering technique on Si wafers. After implantation at room temperature with 400 keV Ar ions and for a fluence of around 10^{15} ions/cm^2, the Mo films exhibit circular damage homogeneously dispatched all over the whole sample (Goudeau et al., 2004). Similar buckles were also observed on Au 100 nm thick films on Si wafers after H implantations (Eren et al., 2014). These circular structures are quite complex but really similar to the ones shown in Fig. 6 (upper left side of the mapping). In this experimental case, $D/h \approx 25$ and the initial stresses (*i.e*. before implantation) were estimated by curvature Stoney method to be approximately $\sigma_0 = 2$ GPa in compression, leading to $\sigma_0/E = 7.10^{-3}$. As these structures are energetically stable only for very low σ_0/E values (see Fig. 7), our numerical results strongly support the idea that the implantation process may also result in a strong decrease of the internal stresses in the films (Goudeau et al., 2004).

4. Conclusions

Circular ring-shaped buckles with undulating edges have been experimentally observed by optical, atomic force and scanning electron microscopy on Ta 240 nm thick films deposited on silicon wafers. It is shown that these specific buckles (1) are only evidenced for high diameters and (2) exhibit a polygonal area in their middle, those number of sides increases with the increasing diameter. Finite elements simulations confirm that wavy ring-shaped buckles are only energetically favorable above a critical diameter and result from the pressure mismatch between the inside and outside parts of the buckles. An internal stress threshold has been evidenced, below which some more complex non-axi-symmetrical buckles are observed. At a given diameter, the increase of stress decreases the polygonal character (number of sides) of the middle part pressed down to the substrate. Contrary to what was previously shown on smooth (*i.e.* without edge undulations) circular blisters, plastic events were evidenced by finite element simulations not to be a key-parameter for wavy ring-shaped buckles to appear, even if sometimes experimentally observed. It is believed that the edge undulations play a

similar role to stabilize the ring-shaped buckles for high diameters.

Acknowledgments.

This work was partially supported by the National Natural Science Foundation of China (Grant No. 91963123), the Ten Thousand Talents Plan of Zhejiang Province of China (No. 2018R52003), and the Fundamental Research Funds for the Provincial University of Zhejiang (No. GK199900X022).

Figure captions

Figure 1. Optical micrographs of tantalum 240 nm thick films sputter-deposited on silicon wafer. (a) Overview showing the large variety of buckled morphologies (b) Superimposed buckles exhibiting both smooth and wavy edges.

Figure 2. Characteristic buckles for increasing diameter *D*. (a) Circular buckle with smooth edges (b) Ring-shaped buckle with smooth edges (c) Circular buckles with wavy edges (d) Bone-like buckles (e,f) horseshoe-like buckles (g-i) Ring-shaped buckles with wavy edges.

Figure 3. Spontaneous transition from (a) a wavy circular buckle to (b) a wavy ring-shaped buckle. The time interval between is 270 days. The transition is characterized by a collapse of the film at the center of the buckle, down to the substrate.

Figure 4. Experimental morphological parameters of the buckles. (a) normalized maximum deflection δ/D, (b) petal number N and (c) period of the edge undulations λ, as a function of D.

Figure 5. FEM configuration. z is the out-of-plane displacement of the film. D is the diameter of the fixed debonded area between the film and the elastically hard substrate. The size of the box is $L_x=L_y=3D$.

Figure 6. FEM morphological mapping of a circular plate as a function of the internal stress σ_0 and the pressure mismatch Δp, for h = 240 nm, D = 120 μm, E = 186 GPa and ν = 0.35.

Figure 7. FEM morphological mapping of a circular plate as a function of normalized stress σ_0/E and normalized diameter D/h, for Δp = 1 atm and for ν = 0.35.

Figure 8. Damage circular structures on Mo 200 nm thick films implanted by Ar ions (AFM investigation).

References

Abdallah A.A., Kozodaev D., Bouten P.C.P., den Toonder J.M.J., Schubert U.S., de With G., Buckle morphologt of compressed inorganic thin layers on a polymer substrate, Thin Solid Films 2006;503:167.

Abdallah A.A., Bouten P.C.P., den Toonder J.M.J., de With G., The effect of moisture on buckle delamination of thin inorganic layers on a polymer substrate, Thin Solid Films 2008;516:1063.

Argon A.S., Gupta V., Landis H.S., Cornie J.A., Intrinsic Toughness of Interfaces, Materials Science and Engineering A 1989;107:41.

Audoly B., Roman B., Pocheau A., Secondary buckling patterns of a thin plate under in-plane compression, Eur. Phys. J. B 2002;27:7.

Chen S.L., Zhao Y.A., Shao J.D., Wang Y.Z., Fang Z., Liu X.F., Hu G.H., Leng Y.X. Xu Y., Ultra short laser driven stable buckling of blisters in chirped mirror, Appl. Phys. Lett. 2013;102:081605.

Cordill M.J.,. Moody N.R, Bahr D.F., The effects of plasticity on adhesion of hard films on ductile interlayers, Acta Mater. 2005;53:2555.

Cordill M.J., Bahr D.F., Moody N.R., Gerberich W.W., Adhesion measurements using telephone cord buckles, Mater. Sci. Eng. A 2007;443:150.

Cordill M.J., Fisher F.D., Rammerstorfer F.G., Dehm G., Adhesion energies of Cr thin films on polyimide determined from buckling: experiment and model, Acta Materialia 2010;58:5520.

Coupeau C., George M., Regache I., Colin J., Grilhé J., Buckling pattern with rings: an evidence of plastic damage in thin films, Phil. Mag. Lett. 2003;83:453.

Coupeau C., Grilhé J., Dion E., Dantas de Morais L., Colin J., Evidence of vacuum between buckled films and their substrates, Thin Solid Films 2010;518:5233.

Coupeau C., Parry G., Colin J., David M.-L, Labanowski J., Grilhé J. Kinetic evolution of blistering in hydrogen-implanted silicon, Applied Physics Letters 2013;103:031908.

Coupeau C., Boijoux R., Ni Y., Parry G., Interacting straight-sided buckles: an

enhanced attraction by substrate elasticity, J. Mech. Phys. Solids 2019;124:526.

Eren B., Marot L., Gunzburger G., Renault P-O, Glatzel Th., Steiner R., Meyer E., Hydrogen-induced buckling of gold films, J. Phys. D: Appl. Phys. 2014 ;47 :025302.

Evans A.G., Hutchinson J.W., On the mechanics of delamination and spalling in compressed films, Int. J. Solids Struct. 1984 ;20 :455.

Faou J.-Y., Parry G., Grachev S., Barthel E., How does adhesion induce the formation of telephone cord buckles, Phys. Rev. Lett. 2012;108:116102.

Faou J.-Y., Grachev S., Barthel E., Parry G., From telephone cords to branched buckles: a phase diagram, Acta Mater. 2017;125:524.

Gioia G., Ortiz M., Delamination of compressed thin films, Adv. Appl. Mech. 1997;33:119.

Goudeau P., George M., Coupeau C., Ion irradiation effects on the mechanical stability of compressed metallic, Appl. Phys. Lett. 2004 ;84 :894.

Grachev S.Y., Mehlich A., Kamminga J.D., Barthel E., Sondergard E., High-throughput optimization of adhesion in multilayers by superlayers gradients, Thin Solid Films 2010;518:6052.

Guo T., He J., Pang X., Volinsky A.A., Su Y., Qiao L., High temperature brittle film adhesion measured from annealing induced circular blisters, Acta Mat. 2017;138:1.

Hamade S., Durinck J., Parry G., Coupeau C., Cimetière A., Grilhé J., Colin J., Effect of plasticity and atmospheric pressure on the formation of donut-and croissant-like buckles, Phys. Rev. E 2015;91:012410.

Hutchinson J.W., Thouless M.D.,. Liniger E.G, Growth and configurational stability of circular, buckling-driven film delaminations, Acta Metall. Mater. 1992;40:295.

Hutchinson J.W., Suo Z., Mixed mode cracking in layered materials, Adv. Appl. Mech. 1992;29:63.

Kleinbichler A., Pfeifenberger M.J., Zechner J., Wöhlert S., Cordill M.J., Scratch induced thin film buckling for quantitative adhesion measurements, Materials & Design 2018;155:203.

Kuznetsov A.S., Gleeson M.A., Bijkerk F., Hydrogen induced blistering mechanisms in thin coatings, Journal of Physics: condensed matter 2012;24:052203.

Lamri S., Langlade C., Kermouche G., Martinez V., Estimation of the stress relief induced in CrN thin films by buckling, Mat. Science Eng. A 2010;527:7912.

Jin H., Lu W.Y., Cordill M.J., Schmidegg K., In situ study of cracking and buckling of chromium films on PET substrates 2011 ;51 :219.

Lee K., Lee S., Khang D.Y., Lee T., Wrinkling evolution of a growing bubble: the wonders of petal-like patterns in amorphous silicon membranes, Soft Matter 2010;6:3249.

Marot L., De Temmerman G., van den Berg M.A., Renault P.-O., Covarel G., Joanny M., Travère J.M., Steiner R., Mathys D., Meyer E., ITER first mirror mock-ups exposed in Magnum-PSI, Nucl. Fusion 2016 ;56 :066015.

McDonald J.P., Mistry V.R., Ray K.E., Y. S.M., Nees J.A., Moody N.R., Femtosecond laser induced delamination and blister formation in thermal oxide films on silicon (100), Appl. Phys. Lett. 2006 ;88 :153121

Moller J., Reiche D., Bobeth M., Pompe W., Observation of boron nitride thin film delamination due to humidity, Surface Coating Tech. 2002 ;150 :8.

Moon M.-W., Jensen H.M., Hutchinson J.W., Oh K.H., Evans A.G., The characterization of telephone cord buckling of compressed thin films on substrates, J. Mech. Phys. Solids 2002;50:2355.

Moon M.-W., Chung J.W., Lee K.R., Oh K.H., Wang R., Evans A.G., An experimental study of the influence of imperfections on the buckling of compressed thin films, Acta Mater. 2002;50:1219.

Moon M.-W., Lee K.R., Oh K.H., Hutchinson J.W., Buckle delamination on patterned substrates, Acta Mater. 2004;52:3151.

Ni Y., Yu S.-J., Jiang H., He L., The shape of telephone cord blisters, Nat. Commun. 2017;8:14138.

Parry G., Coupeau C., Colin J., Cimetière A., Grilhé J., Buckling and post-buckling of stressed straight-sided wrinkles: experimental AFM observations of bubbles formation and finite element simulations, Acta Mater. 2004;52:3959.

Parry G., Cimetiere A., Coupeau C., Colin J., Grilhé J.. Stability diagram of unilateral buckling patterns of strip-delaminated films, Phys. Rev. E 2006;74:066601.

Parry G., Coupeau C., Dion E., David M.-L., Colin J., Grilhé J., About the internal pressure in cavities derived from implantation-induced blistering in semi-conductors, Journal of Applied Physics 2011;110:114903.

Peponas S., Guedda M., Benlahsen M., On the post-contamination effect on the delamination of sputtered amorphous carbon nitride films, Solid State Comm. 2008;146:78.

Pundt A., Pekarski P., Buckling of thin niobium-films on polycarbonate substrates upon hydrogen loading, Scripta Materialia 2003;48:419.

Volinsky A.A., Moody N.R., Gerberich W.W., Interfacial toughness measurements for thin films on substrates, Acta Mater. 2002;50:441.

Volinsky A.A., Experiments with in-situ thin film telephone cord buckling delamination propagation, Mat. Res. Soc. Symp. Proc. 749 (2003) W10.7.1–W10.7.6.

Wang J.S., Evans A.G., Measurements and analysis of buckling and buckle propagation in compressed oxyde layers on superalloy substrates, Acta Mater. 1998;46:4993.

Waters P., Volinsky A.A., Stress and moisture effects on thin film buckling delamination, Experimental mechanics 2007;47:163.

Yan Y., Wang B., Yin J., Wang T., Chen X., Spontaneous wrinkling pattern of a constrained thin film membrane, Appl. Phys. A 2012;107:761.

Yu H.Y., Kim C., Sanday S.C., Buckle formation in vacuum-deposited thin films, Thin Solid Films 1991; 196:229.

Yu S.-J., Xiao X.F., Chen M.G., Zhou H., Chen J., P.Z. Si, Z.W. Jiao, Morphological selections and dynamical evolutions of buckling patterns in $SiAlN_x$ films: from straight-sided to telephone cord or bubble structures, Acta Mater. 2014;64:41.

Yu S.-J., Zhang Y.J., Chen M.G., Telephon cord buckles in wedge-shaped Fe films sputtering deposited on glass substrates, Thin Solid Films 2009;518:222.

Zhou H., Ma L., Yu S.-J., Ni Y., Ring-shaped buckles in metal films induced by evaporation of micro-scaled silicone oil droplets, Thin Solid Films 2018;651:131.

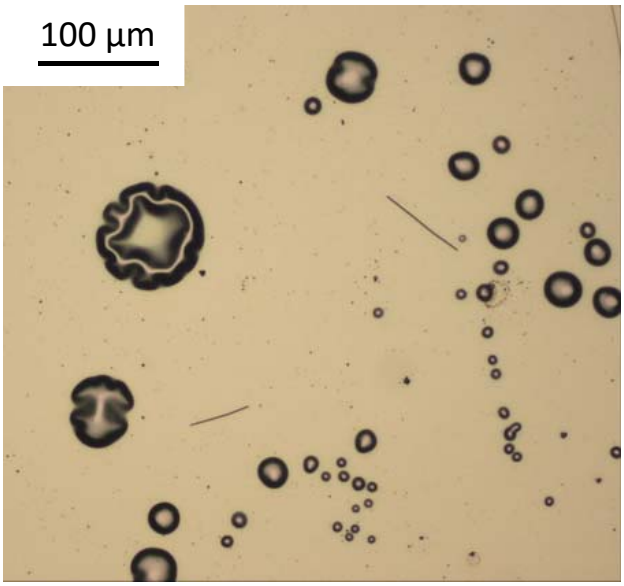

(a)

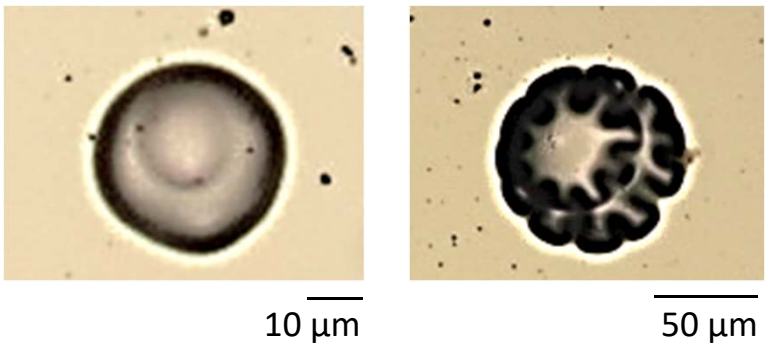

(b)

FIGURE 1

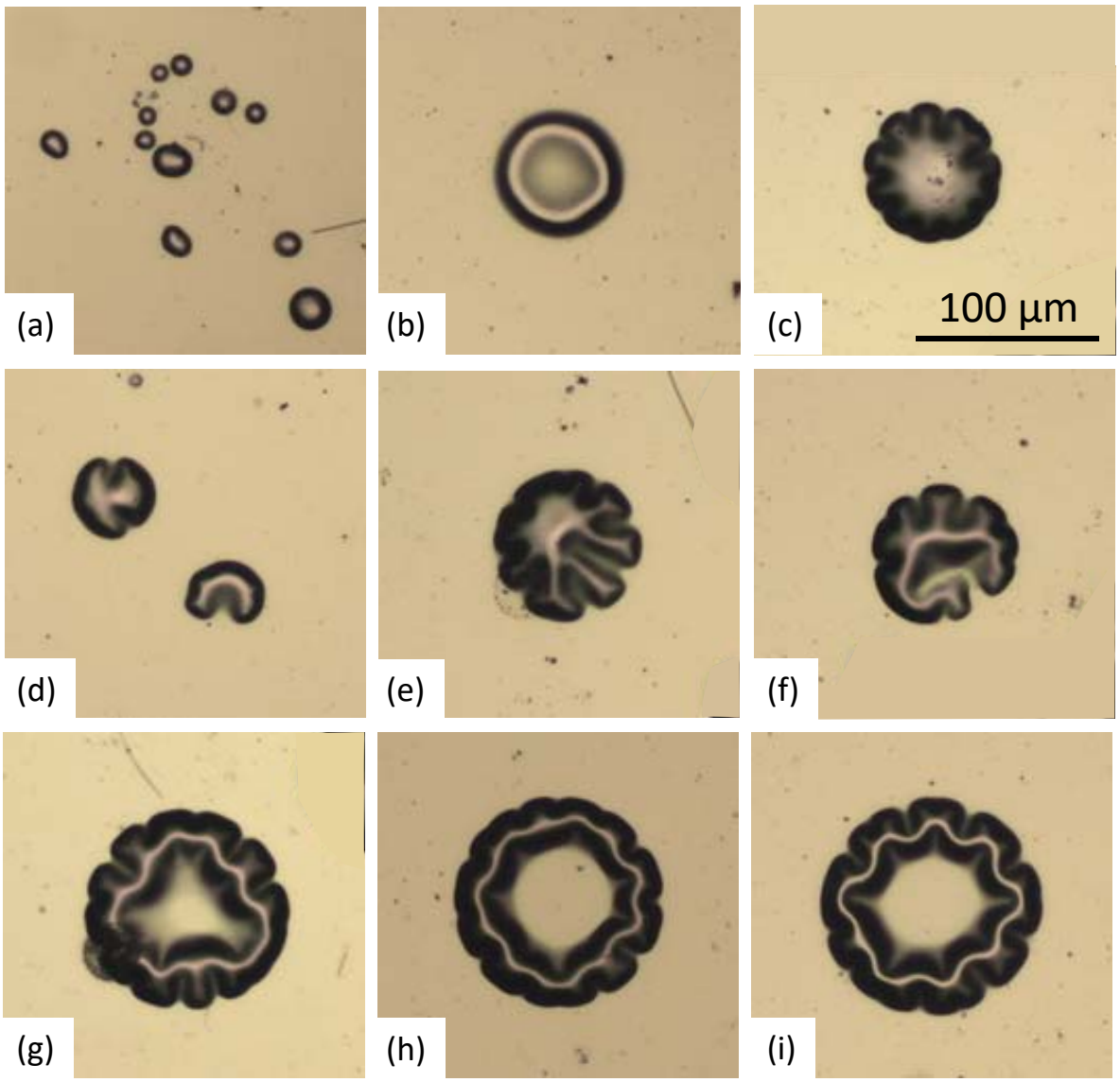

FIGURE 2

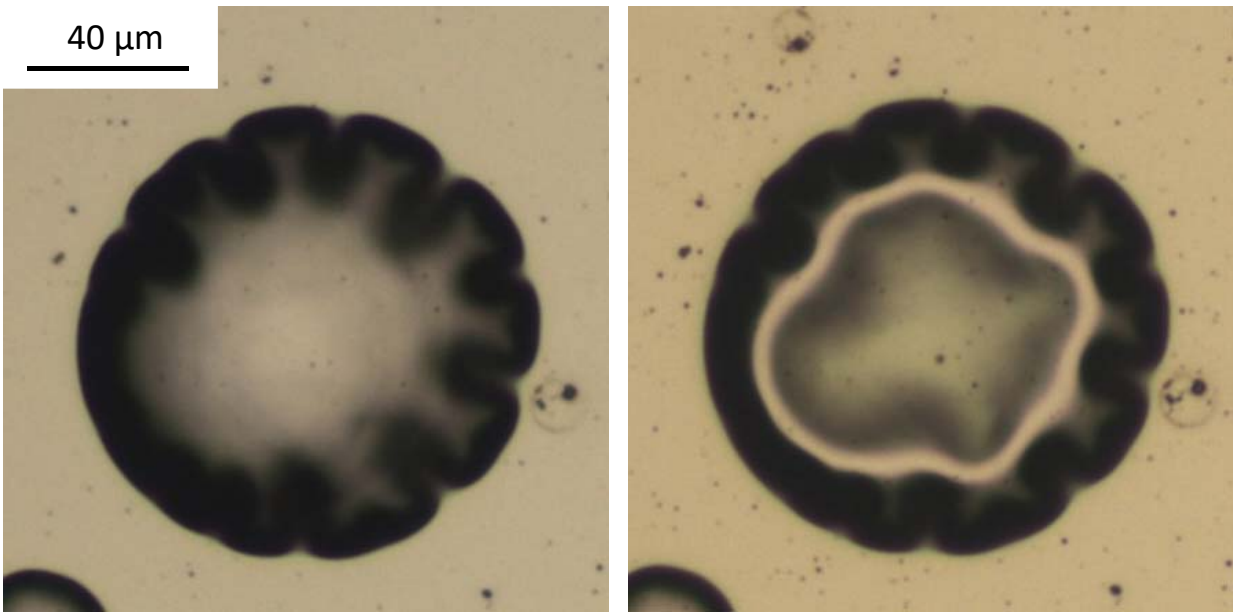

(a) (b)

FIGURE 3

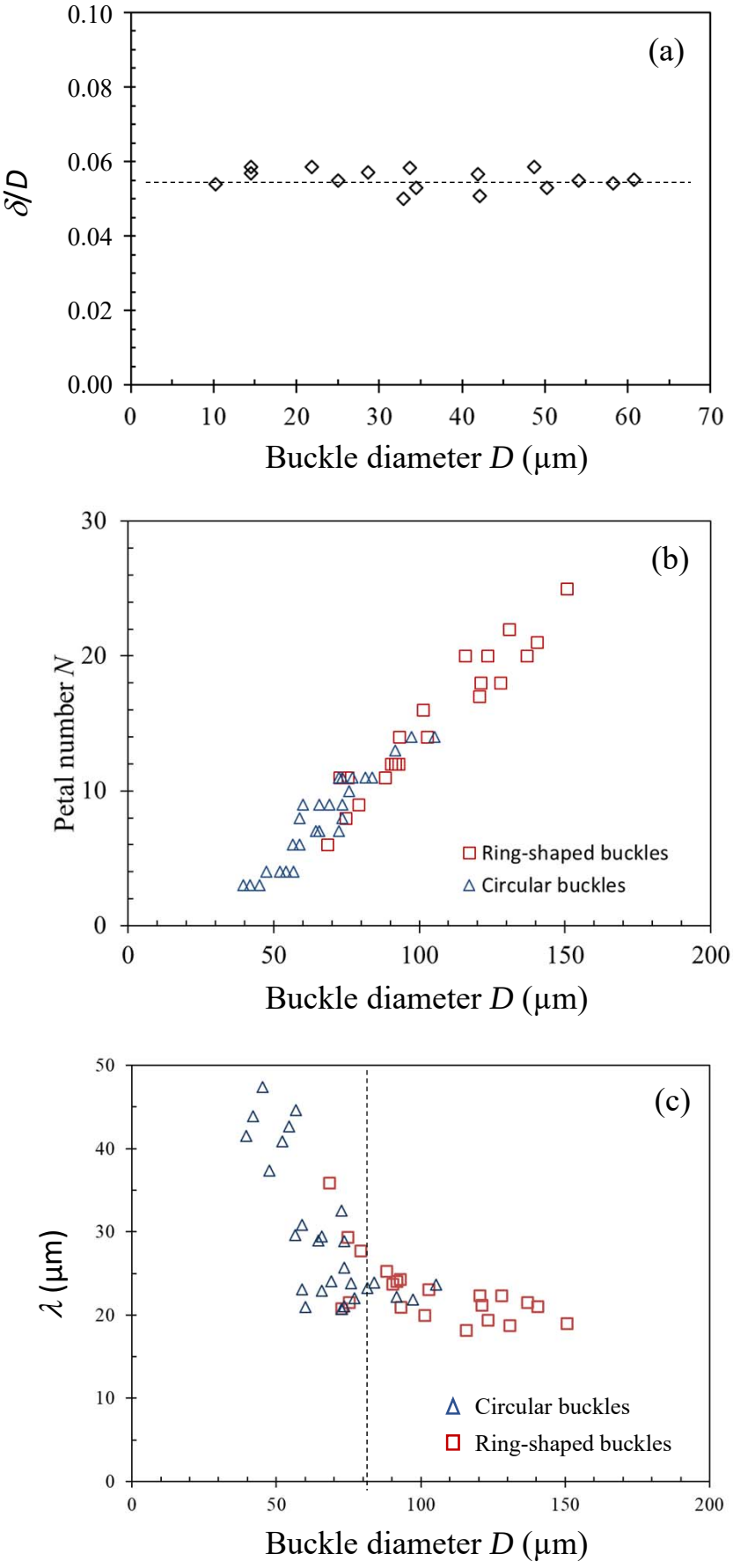
(a)
δ/D
0.10
0.08
0.06
0.04
0.02
0.00
0
10
20
30
40
50
60
70
Buckle diameter D (μm)
(b)
Petal number N
30
20
10
0
0
50
100
150
200
Ring-shaped buckles
Circular buckles
Buckle diameter D (μm)
(c)
λ (μm)
50
40
30
20
10
0
0
50
100
150
200
Circular buckles
Ring-shaped buckles
Buckle diameter D (μm)

FIGURE 4

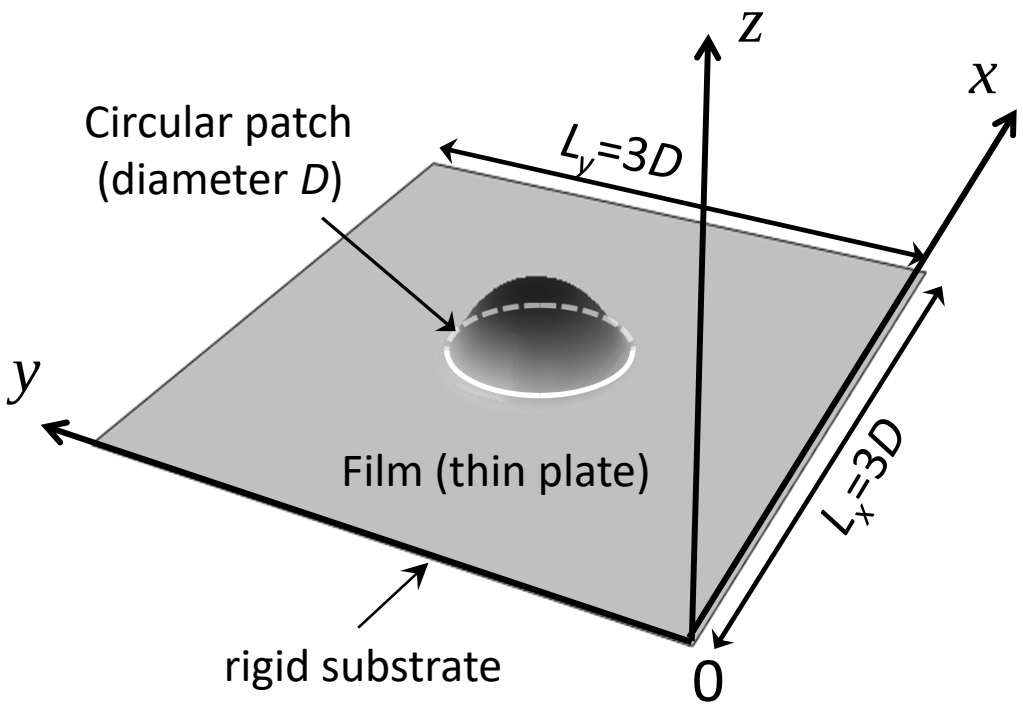
z
x
Circular patch
(diameter D)
L_y=3D
y
Film (thin plate)
L_x=3D
rigid substrate
0

FIGURE 5

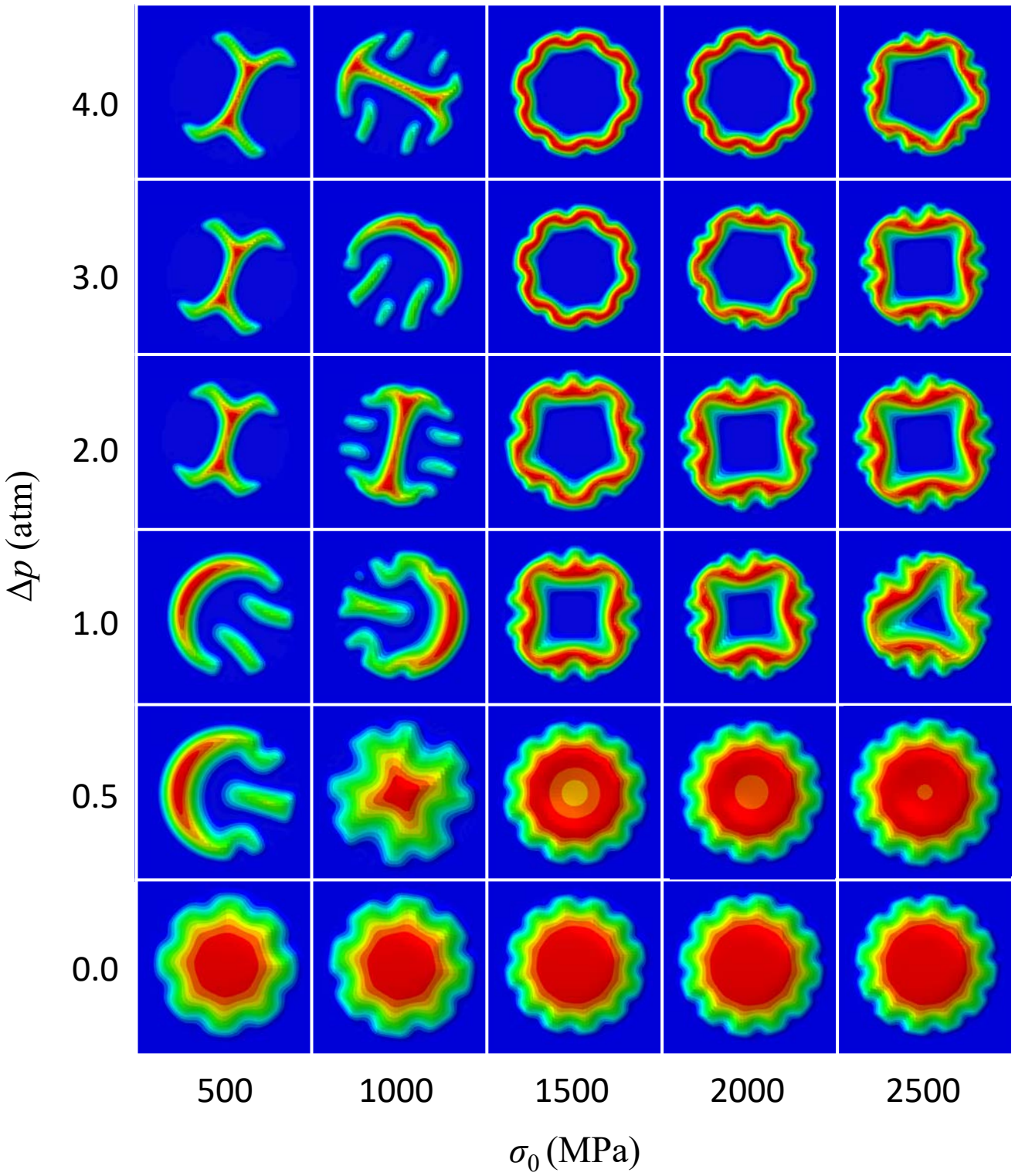

FIGURE 6

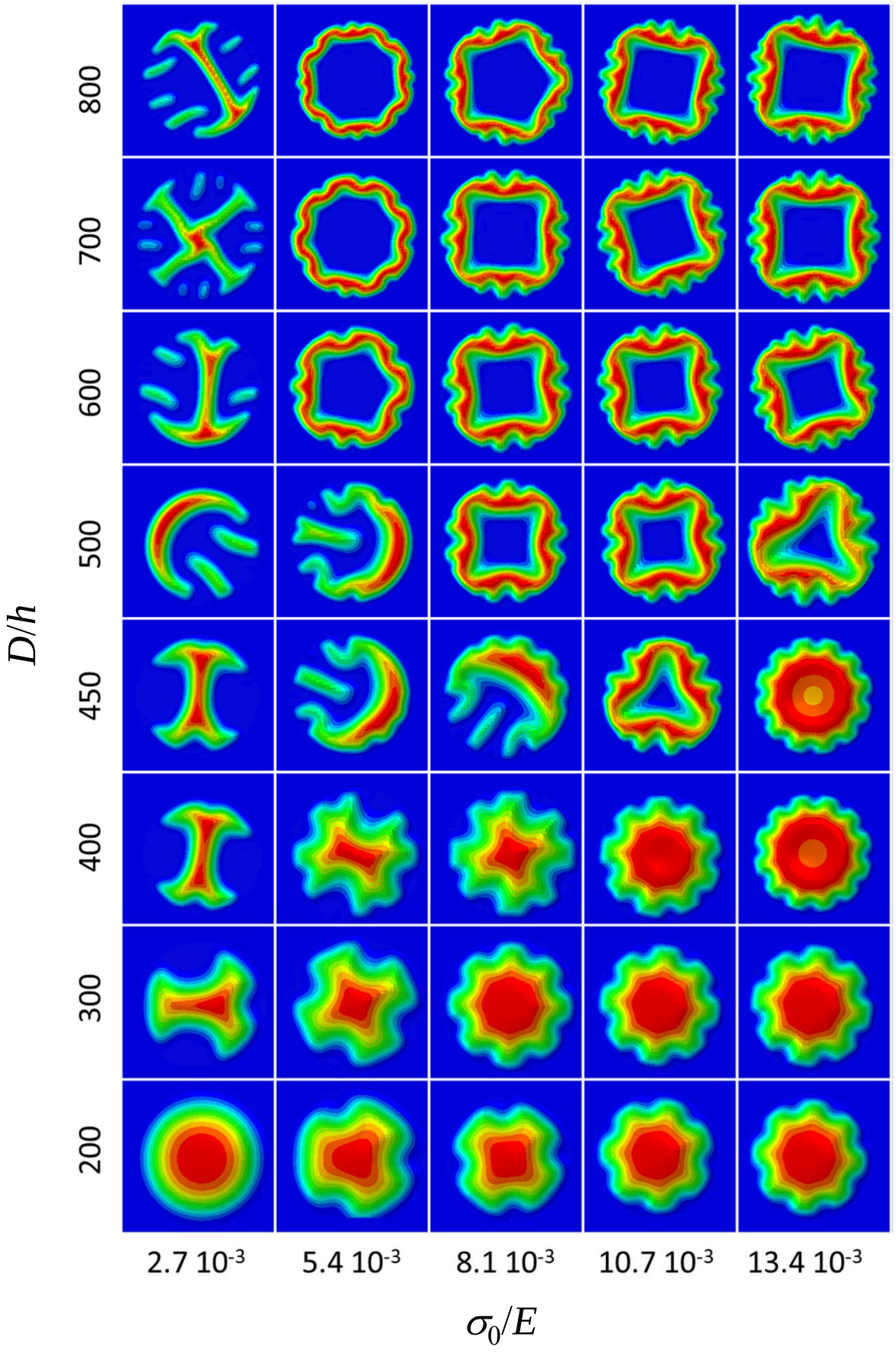
D/h
800
700
600
500
450
400
300
200
2.7 10-3
5.4 10-3
8.1 10-3
10.7 10-3
13.4 10-3
σ0/E

FIGURE 7

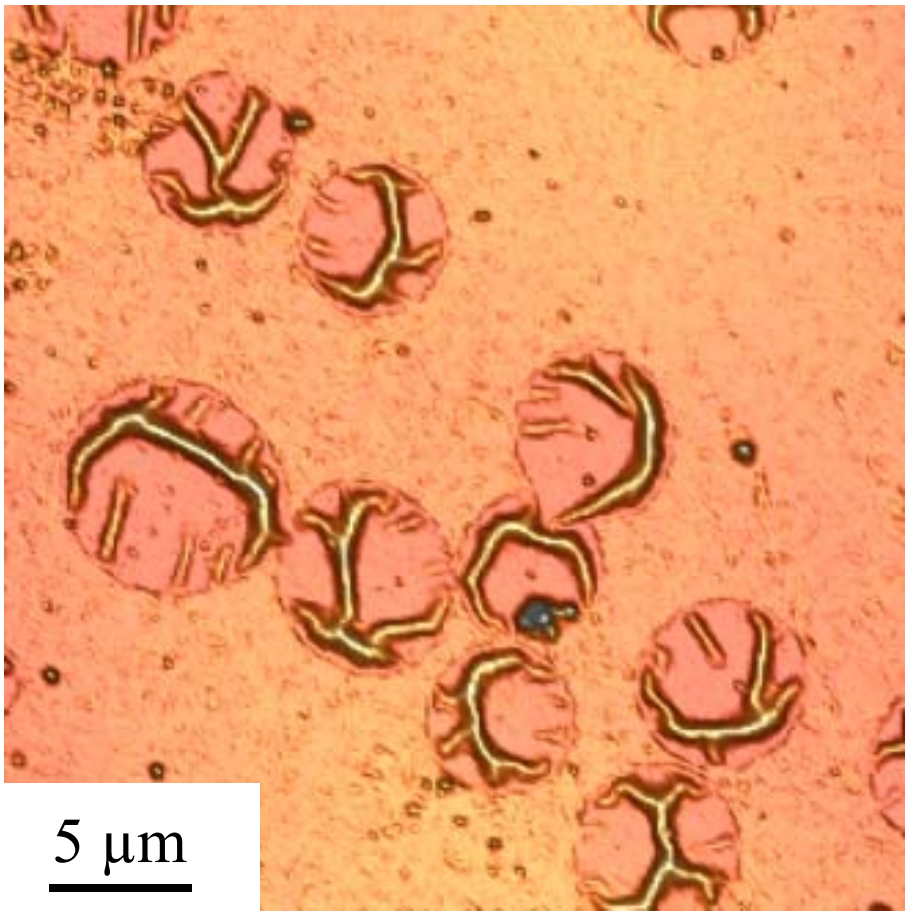

FIGURE 8

MORPHOLOGICAL MAPPING OF CIRCULAR BLISTERS TAKING INTO ACCOUNT A PRESSURE MISMATCH BETWEEN BOTH SIDES OF THE BUCKLED FILM

Simulation results
taking into account a pressure mismatch of 1 atm
(Finite elements)

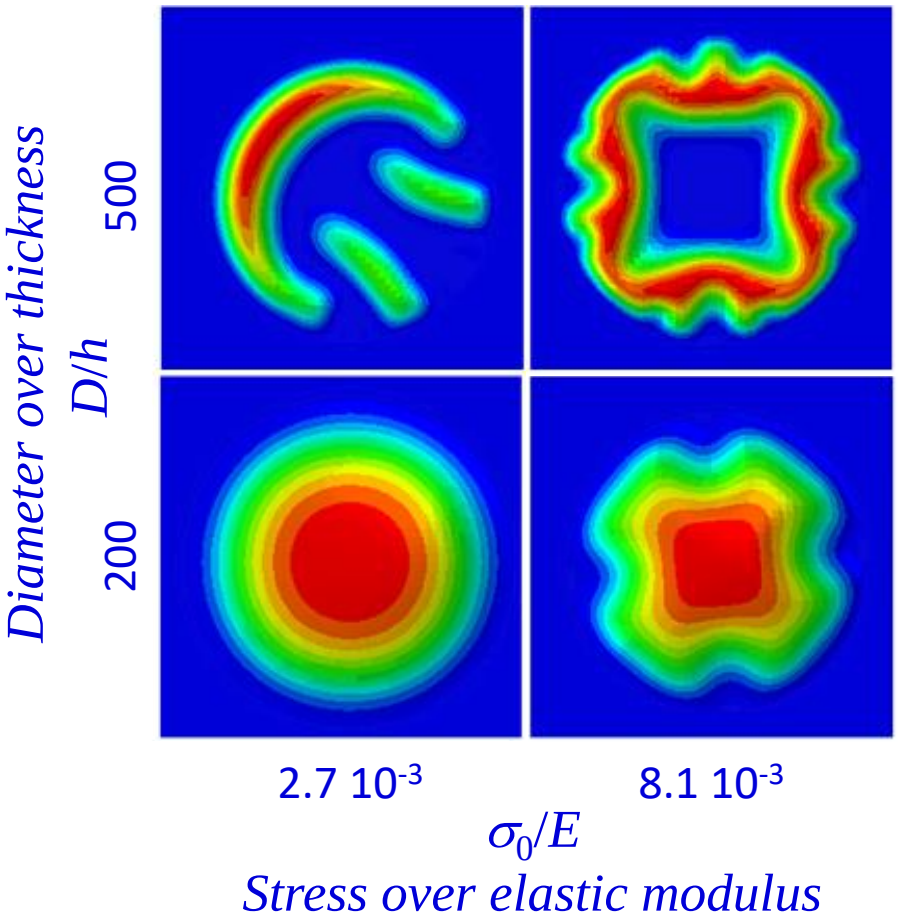

Experimental results:
240 nm thick Ta films on Si wafers
(optical micrograph)